JOURNAL OF CATALYSIS 103, 436–449 (1987)

A High-Resolution Electron Microscopy Study of Photodeposited Pd Particles on TiO_2 and Their Oxidation in Air

J. W. M. JACOBS* AND D. SCHRYVERS†

*Philips Research Laboratories, 5600 JA Eindhoven, The Netherlands, and †Electron Microscopy Centre for Materials Research, University of Antwerp, RUCA, Groenenborgerlaan 171, B-2020 Antwerp, Belgium

Received April 10, 1986; revised September 2, 1986

Small (1- to 20-nm) photodeposited Pd particles on thin polycrystalline TiO_2 films were examined by conventional and high-resolution electron microscopy (HREM). Lattice imaging in these particles and optical diffraction analysis showed that the particle structure was face centered cubic (fcc) and that the lattice parameters were expanded up to 10% with respect to the bulk value. When the samples were heated under high vacuum at 500°C for 1 h, lattice expansions up to 5% were observed. In this case all Pd agglomerates (>4 nm), consisting of randomly oriented 2- to 4-nm Pd clusters which are fused together, recrystallized into spherical Pd monocrystallites. Heating in air at 500°C for 1 h brought about an increase in the maximum lattice expansion up to 15% and in almost all particles a distortion of the fcc structure. Furthermore various other lattice defects such as lamellar twins, stacking faults, dislocations, and lattice bending were observed. Some observations also suggested an enhanced Pd–TiO_2 interaction. Prolonged oxidation up to 24 h revealed images that could be explained by a phenomenon which was recently described as pit formation in the center of Pd crystallites. In only a few cases did lattice imaging indicate the possible presence of stoichiometric PdO. It is suggested that the dissolution of oxygen in the bulk of the Pd particles is the main explanation of our observations.

INTRODUCTION

Photodeposited metal particles on a TiO_2 support are used as catalytic centers in light-energy storage systems (*1*) and in photographic imaging systems (*2, 3*). Catalytic reactions in such systems may be sensitive to the atomic structure of the metal particles. One important structural factor connected with photodeposited metal is the oxidation state of the metal. In the case of Pt photodeposition from aqueous H_2PtCl_6 solutions containing acetate ions, some controversy exists about the Pt oxidation state (*4–7*). The reported states vary between zero (pure metallic Pt) (*4*) and a mixture of oxidation states II and IV (no metallic Pt) (*5*).

Recently we undertook a detailed transmission electron microscopy (TEM) investigation of the process of Pd photodeposition on thin polycrystalline TiO_2 films (*8*). Using a newly developed specimen preparation technique (*9*) for high-resolution electron microscopy (HREM) it was shown that millisecond UV illumination of a TiO_2 film immersed in an aqueous palladium chloride solution produced very small (<4 nm) Pd clusters on the TiO_2 surface.

Pd clusters produced by this technique can be used directly as catalytic centers for the initiation of electroless metal deposition (*2*). Pd clusters may catalyze the anodic oxidation of the reducing agent in an electroless solution. However, under some experimental conditions the Pd clusters appear to be completely inactive in electroless solutions. For example, it will be reported (*10*) that the size and morphology of Pd clusters did not change during a 2-h residence in an electroless Cu solution after they had previously been exposed to air at room temperature, i.e., the TiO_2 surface was allowed to dry completely before it was immersed in the electroless Cu solution. This observation suggested that the oxidation state of Pd atoms in a Pd cluster might be important in determining the catalytic activity.

0021-9517/87 $3.00

In connection with the foregoing an HREM study of photodeposited Pd particles was carried out in order to obtain direct information about their atomic structure. Direct imaging of lattice planes has already proved to be a versatile technique to obtain information on the crystallographic structure of small metal particles (e.g., (*11–15*)). The use of TEM, however, creates the following major problem: Oxidized Pd atoms possibly present may be reduced in the electron microscope. Thus, for example, if a lattice image of a Pd cluster indicates a metallic fcc structure one must allow for the possibility that this cluster was in an oxidized form before it entered the microscope. One may exclude this possibility if lattice images of clusters reveal a Pd oxide structure, since then it is proved that these clusters are stable in the reducing environment of the microscope.

In order to study the sensitivity of photodeposited Pd clusters for oxidation, Pd/TiO_2 TEM specimens were subjected to high-temperature treatments in air or high vacuum (HV). This paper presents an account of observed lattice images in fcc Pd particles and (partly) oxidized Pd particles.

METHODS

Details about the preparation of TEM specimens and the experimental set-up for illuminations have been given in previous papers (*8, 9*) and are reviewed here briefly.

The TEM specimens consist of a thin (thickness <10 nm) polycrystalline TiO_2 (anatase) film on an amorphous Si_3N_4 membrane (size 15 × 15 μm^2, thickness 13 nm) supported by a small section of a (100) Si wafer (size 1.6 × 1.6 mm^2, thickness 0.38 mm). The TiO_2 film consists of one single layer of 10- to 25-nm anatase grains and is thus optimally structured with respect to the requirement that TEM contrasts from metal clusters deposited on this film can easily be recognized and distinguished from TEM contrasts originating from the TiO_2/Si_3N_4 structure. Lattice images in the TiO_2 grains with a resolution down to 0.19 nm already showed the possibility of HREM work (*9*).

Illumination was carried out with a UV (Ar^+) laser beam (Spectra Physics 165-09, wavelength 351.1–363.8 nm) which was focused (spot size ≈ 13 μm) onto the TiO_2 film by an achromatic convergent lens. Illumination was started 10 min after the TEM specimen was immersed in a quartz cell which was filled with an aqueous solution containing 5.6×10^{-3} *M* $PdCl_2$ and 1.2×10^{-1} *M* HCl. The results presented below were obtained from a number of differently illuminated specimens. The observed characteristic features showed little or no dependence upon the illumination conditions. Light intensities and total illumination times (Δt) were varied between 16 × 10 and 1.6×10^3 W/cm^2 and between 1 ms and 100 ms, respectively. Some samples were illuminated with more than 1 pulse (for example, 10 pulses of 1 ms with intervals of 5 s).

After illumination the specimen was immediately taken from the solution and rinsed as follows: a 1-min dip in water, a 1-min dip in 0.4 *M* aminoacetic acid (pH = 3.8), and finally a 1-min dip in water (*8*). All solutions were prepared from triply distilled water; the illuminations were carried out at room temperature and no gas was bubbled through the Pd plating solution.

In order to oxidize the photodeposited Pd particles the TEM specimens were heated in a quartz tube in air at 500°C for 1 or 24 h. TEM specimens were also high-vacuum annealed in a turbo-molecular pumped system at 500°C for 1 h. The samples were mounted on a molybdenum holder which could be heated by electron bombardment on the back side. The temperature was monitored with a thermocouple and computer controlled. During annealing the pressure in the system remained below 10^{-5} Pa.

HREM investigations were carried out with a JEOL 200CX (operated at 200 kV in top-entry stage) and a Philips EM 430ST (operated at 300 kV) transmission electron microscope. The time which passed be-

tween sample preparation and subsequent inspection in the microscope varied between 1 h and 1 week. However, no changes in the TEM specimens due to these varying room temperature exposures to laboratory air were observed.

Optical diffraction was used to analyze the recorded micrographs and corresponded to direct microdensitometrical measurements. The diffractometer was equipped with an adjustable diaphragm to obtain optical diffraction patterns of individual particles. The (101) lattice spacings of 0.352 nm in the anatase monocrystallites, which appeared in almost all micrographs, provided a direct calibration of image magnification. Care was taken to ensure that the laser beam was transmitted perpendicularly through the TEM negative plate. However, the measured distances and angles were not sensitive to slight optical misalignments in the diffractometer. Thus it was estimated that the reported lattice distances and angles between lattice planes in (oxidized) palladium particles could be measured with an accuracy of 2% or better. The measured distances are averages since non-uniform lattice relaxations may occur in small metal particles. Furthermore it is noted that, due to the elongation of the reciprocal lattice points for a very thin particle, the spacing between lattice fringes can be affected. From an estimate of the particle thickness (e.g., spherical particles) it was calculated that a slight misalignment of the electron beam in the microscope could not produce errors in the measured distances larger than the mentioned accuracy.

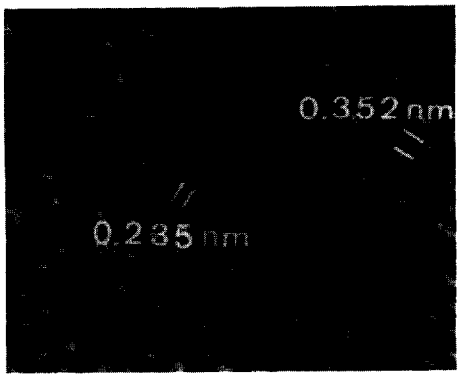

FIG. 1. A 2-nm Pd cluster (no heat treatment) showing expanded (111) lattice fringes. Lattice parameters of the Pd cluster and the TiO_2 grain are indicated.

RESULTS

No Heating

Short ($\Delta t < 3$ ms) light pulses produced a number of separate Pd clusters (<4 nm) on the TiO_2 surface. The density of these clusters and their size range were mainly determined by the light intensity and the illumination time, respectively (*8*). Imaging of one set of lattice planes (one-dimensional lattice imaging) was possible when the Pd clusters were larger than 1.5 nm. The lattice phase contrast of smaller Pd clusters could not clearly be resolved against the noisy background structure of the Si_3N_4 support owing to the low number of Pd atoms in these clusters. Figure 1 shows the (111) lattice fringes in a 2-nm Pd cluster which is located close to a TiO_2 grain whose 0.352-nm lattice spacing is also visible. From the corresponding optical diffraction pattern (ODP) a Pd d_{111} lattice parameter is measured (0.235 nm) which is 5% larger than that of bulk Pd (0.225 nm (*16*)).

Direct evidence for the fcc structure in small Pd clusters only comes from two-dimensional lattice imaging which was possible when the Pd clusters were larger than 2.0 nm. The 3.5-nm Pd cluster in Fig. 2a shows a structure image along the (011) zone revealing lattice fringes from the (111) and (200) planes. Although the contrast of the lattice resolution is relatively weak, the fcc character can be recognized from the analysis of the corresponding ODP (Figs. 2b, c). It is noted, however, that the lattice spacings of the (200) and (111) planes (0.213 and 0.234 nm) are increased relatively differently (9 and 4%) with respect to their values in bulk Pd (0.195 and 0.225 nm). The angles between the lattice planes (55 and 70°) correspond to their values in a nondis-

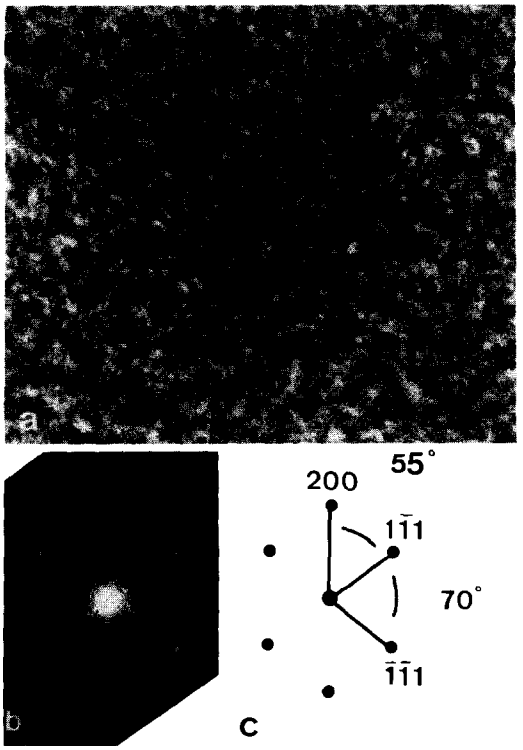

FIG. 2. (a) A 3.5-nm Pd cluster (no heat treatment) showing lattice fringes from the (111) and (200) planes. (b) Optical diffraction pattern (ODP) from (a). (c) Schematic representation of (b) indicating the measured angles.

torted fcc lattice (54.7 and 70.5°) and possible deviations from these values are too small to be measured.

At this point we note that lattice expansions up to 10% occur in all Pd clusters in the 1.5- to 4-nm size range. The possible anisotropy of the lattice expansion (Fig. 2), however, could not clearly be determined in all clusters and more investigations are certainly needed to clear up this problem.

Since the TiO_2 film consists of well-defined monocrystallites we have the opportunity to investigate structural relationships in the interface of a Pd cluster and a TiO_2 crystallite by lattice imaging of the interface (edge on and on top). HREM observations suggest the possible occurrence of epitaxy (*10*).

HREM and dark field imaging showed that almost all small (<4-nm) photodeposited Pd clusters are single crystals. However, some Pd clusters exhibited the phenomenon of twinning, as is shown, for example, in Fig. 3a for a 2.5-nm Pd cluster. A twin boundary parallel to the closely packed (111) planes is visible in the cluster. The ODP (Fig. 3b) again points to an fcc structure with increased averaged spacings of the (111) planes (d_{111} = 0.242 nm; ≈7.5%

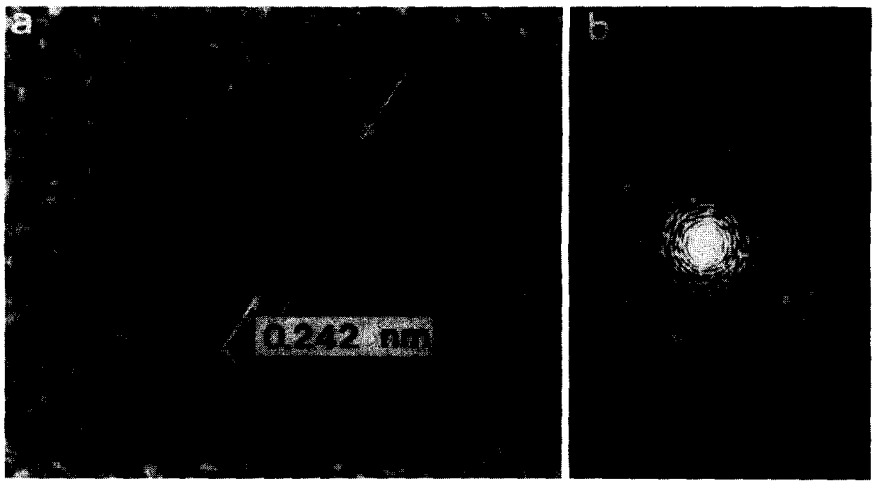

FIG. 3. (a) A 2.5-nm Pd cluster (no heat treatment) showing (111) and (200) lattice fringes and a twin boundary (arrows). (b) ODP from (a).

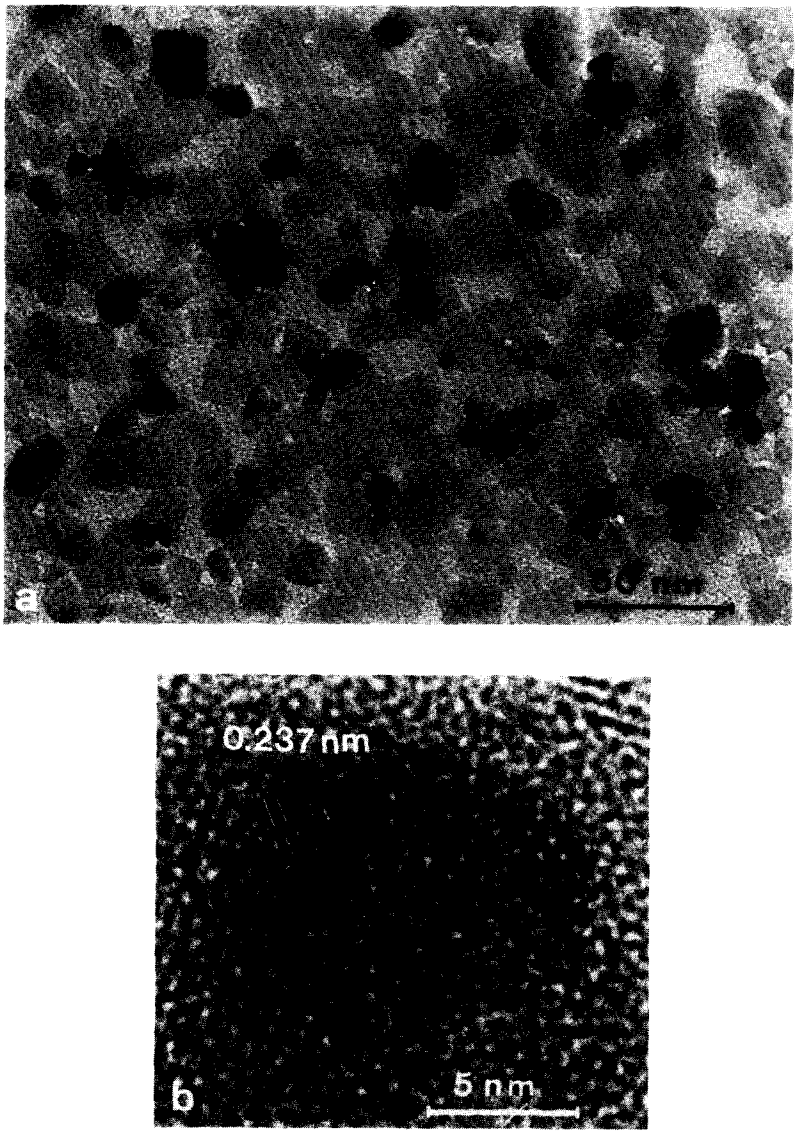

FIG. 4. (a) Pd agglomerates consisting of a number of 2- to 4-nm Pd particles fused together (no heat treatment). (b) Lattice imaging in a 6-nm Pd agglomerate.

expansion). The sharpest diffraction spots (arrows) belong to the set of (111) planes parallel with the twin boundary.

Longer illumination times ($\Delta t > 3$ ms) resulted in the photochemical growth of previously formed 2- to 4-nm Pd clusters. Figure 4a shows a typical example of a distribution of Pd agglomerates (>4 nm) whose growth has taken place by repeated three-dimensional nucleation of 2- to 4-nm Pd clusters (*8*). The agglomerates consist of randomly oriented 2- to 4-nm Pd clusters which are fused together. This is illustrated in Fig. 4b which shows a 6-nm-size Pd agglomerate in which different (111) lattice plane orientations are visible. Similar lattice expansions as mentioned above were observed.

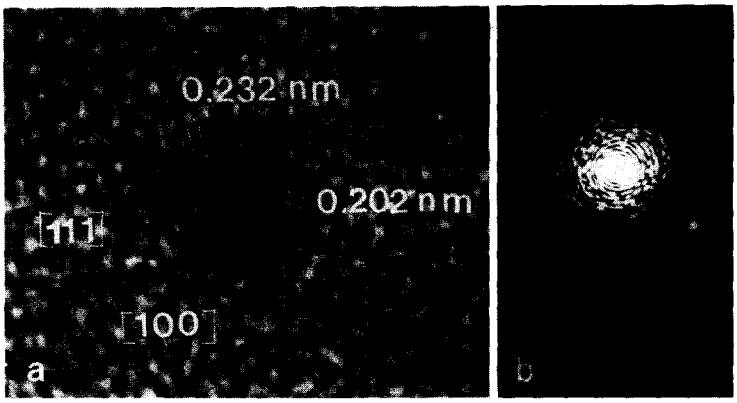

FIG. 5. (a) A 2.5-nm Pd cluster (under HV at 500°C for 1 h) showing lattice fringes from the (111) and (200) planes. (b) ODP from (a).

Heating in High Vacuum at 500°C for 1 h

A HV treatment at 500°C for 1 h did not significantly change the shape of Pd clusters (<4 nm) but had a considerable effect on the structure and morphology of Pd agglomerates (>4 nm).

Lattice expansions up to 5% occurred in all Pd clusters but, unlike the case with non-heated Pd clusters, its anisotropy was too small to be measured. Figure 5a shows a (011) section of a 2.5-nm Pd cluster in which both the (111) and the (200) lattice distances are increased by 3%. Analysis of the ODP (Fig. 5b) shows that the ratio d_{111}/d_{200} approximates to the fcc value of 1.155.

HREM and dark field imaging showed that Pd agglomerates were turned into perfect Pd single crystals with a spherical shape. Figure 6, for example, shows a distribution of spherical Pd particles in the 4- to 8-nm size range.

Heating in Air at 500°C for 1 h

The basic observations when Pd/TiO_2 samples were heated at 500°C for 1 h were the following. The size of Pd clusters or agglomerates was not significantly changed; i.e., phenomena such as sintering,

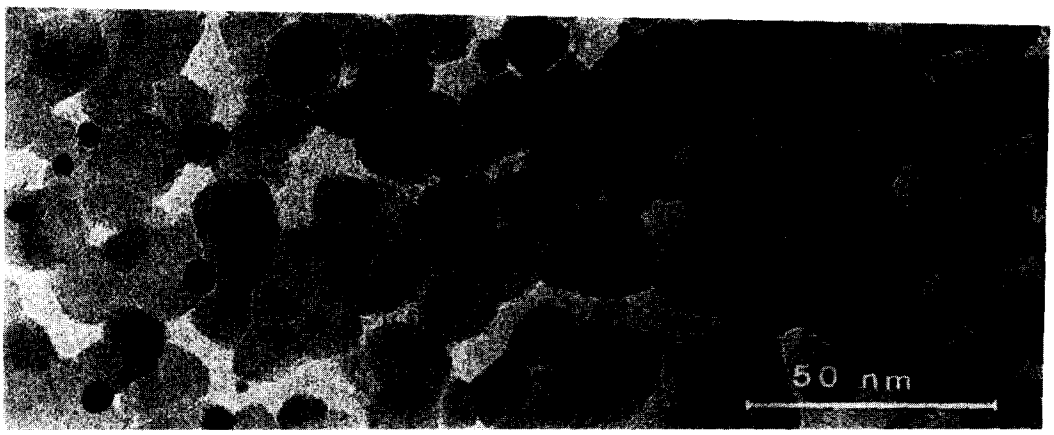

FIG. 6. Spherical Pd particles (under HV at 500°C for 1 h). Illumination conditions during photodeposition were nearly the same as in Fig. 4a.

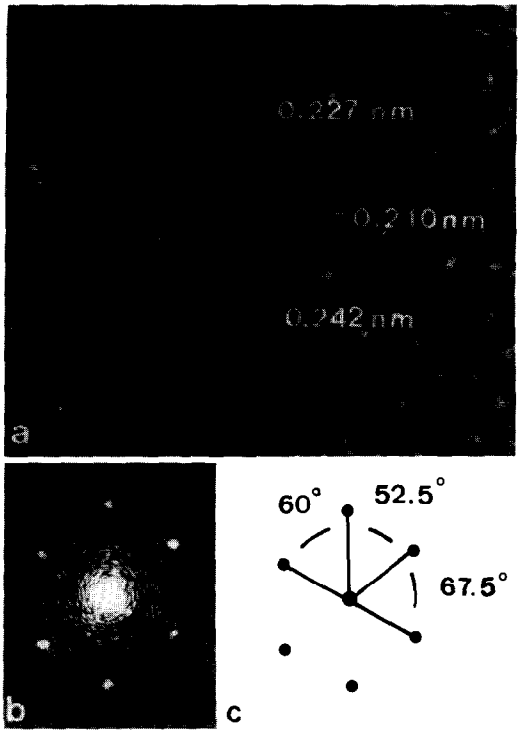

FIG. 7. A 3-nm Pd cluster (in air at 500°C for 1 h) showing two-dimensional lattice imaging. (b) ODP from (a). (c) Schematic representation of (b) revealing angles of a distorted fcc structure.

fragmentation, or rupture were apparently absent. Pd agglomerates still consisted of randomly oriented monocrystalline regions whose size range, however, was changed from about 2–4 nm (no heating) to about 1–5 nm (heating in air). The Pd particles seemed to interact more strongly with the TiO_2 crystallites than before heating. The shape of the Pd particles was slightly changed such that the area of contact between the TiO_2 crystallites and the particles was enlarged (like that shown, for example, in Figs. 9b and 10b).

More importantly, a distortion of the fcc lattice structure was observed in almost all Pd particles. Moreover, lattice expansions up to 15% occurred in all Pd particles. Only in a few cases was there any evidence for a PdO structure (see below).

A characteristic distortion most frequently observed is illustrated in Fig. 7a, which shows two-dimensional lattice imaging in a 3-nm Pd cluster. An analysis of the ODP (Figs. 7b, c) clearly shows a deformation with respect to the symmetrical ODP in Figs. 2b and 5b. The measured angles (60.0, 52.5, and 67.5°) do not correspond to an fcc Pd structure nor to a tetragonal PdO structure (*16*) (in both cases a twofold axial symmetrical ODP should be observed). It should be mentioned that this measured shift of diffraction spots is too large to be attributed to a slight tilt of the view axis with regard to a pure fcc (011) direction. The lattice parameters indicated in Fig. 7a correspond with expanded interplanar distances of (200) and (111) planes in the fcc structure.

Figure 8a shows a Pd particle in which

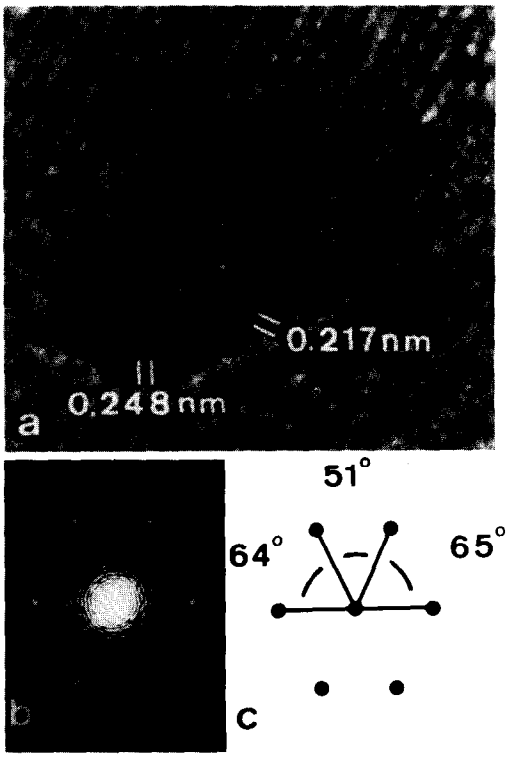

FIG. 8. (a) Pd particle (in air at 500°C for 1 h) showing two-dimensional lattice imaging (left half). (b) ODP from left half of particle in (a). (c) Schematic representation of (b) revealing angles of a distorted fcc structure.

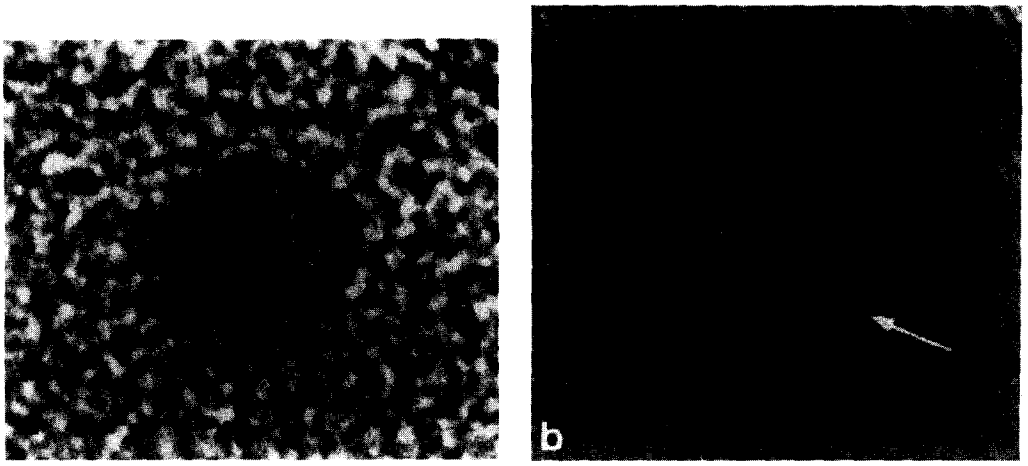

FIG. 9. Planar defects in Pd particles (in air at 500°C for 1 h). (a) A 3.5-nm Pd cluster showing a two-dimensional lattice image. Three lamellar twin boundaries with gap are indicated by arrows. The averaged lattice parameter measured from the ODP is 0.237 nm. (b) A 5-nm Pd particle with stacking fault (arrowed). Note the presence of the TiO_2 crystallite.

one-half shows lattice fringes in two dimensions. The indicated lattice parameters deviate appreciably from the bulk parameters of Pd as well as PdO (*16*). Although the ODP (Fig. 8b) is now symmetric, the measured angles (Fig. 8c) between different reciprocal directions also deviate from simple Pd or PdO values.

Similar distortions to those shown in Figs. 7 and 8 were also observed in Pd agglomerates (>4 nm). From optical diffraction analysis of various fcc distorted lattices it appeared that interplanar distances between (111) planes could vary between 0.225 and 0.260 nm, while marked changes in the angles between simple sets of fcc lattice planes were also observed.

In addition to this characteristic distortion, various other structural deviations from a single-crystalline fcc lattice were observed. Some examples are shown in Figs. 9–11.

Figure 9a shows a 3.5-nm Pd particle in which three lamellar twins (arrows) are visible. The ODP (not shown) only reveals two bright spots together with some weak spots. The bright spots might indicate averaged "(111)-like" vectors (lattice parameter 0.237 nm) in some complicated distorted fcc reciprocal lattice. The presence of the small gaps (darker contrast) in the fringe structure (Fig. 9a) might be associated with twin boundary relaxations (*12*). However, no boundary relaxation could be detected from spot splitting in the ODP (*17*), but this could be due to the insufficient resolution of the optical diffractions. The small change in contrast at the arrows could also be due to a small tilt angle of the electron beam with respect to the plane of the boundaries (*18*).

Figure 9b is an example of a planar defect (arrow) which occurred in a 5-nm particle. The resolution of lattice fringes on both sides of the planar defect indicates a stacking fault. Optical diffraction analysis of this two-dimensional lattice image showed a distorted fcc diffraction pattern similar to those mentioned above.

Figure 10a shows the surprising presence of a stable dislocation (seen clearly by looking along the arrow) in a 3.5-nm Pd particle. An extra lattice plane is visible in the left half of the Pd particle. It is noted that the left side of the Pd particle is in contact with a TiO_2 crystallite which cannot clearly be recognized owing to its low absorption con-

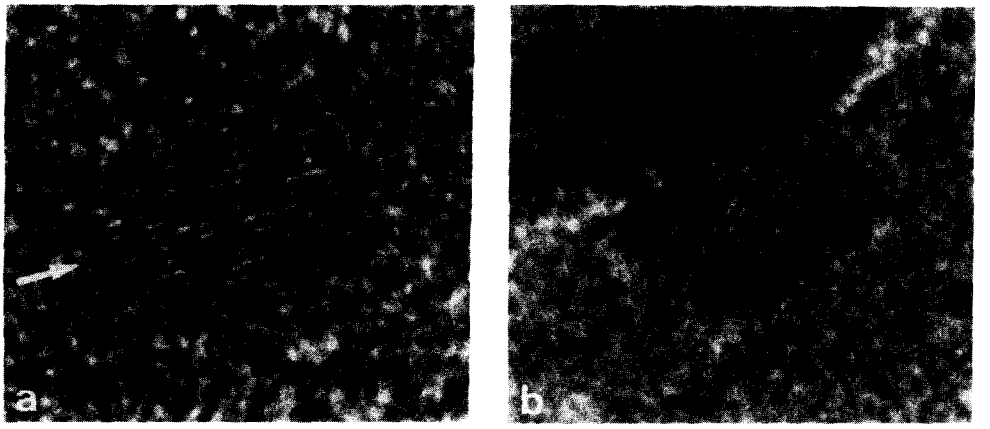

FIG. 10. Lattice fringes in Pd particles (in air at 500°C for 1 h) showing (a) an edge dislocation (arrow) and (b) lattice bending.

trast. Figure 10b shows an example of strain-induced lattice bending in a 3-nm Pd particle (excluding thickness variations in such a small particle). This is further evidence for an enhanced interaction between the Pd particles and the TiO_2 crystallites due to the heat treatment in air.

It appeared that Pd particles larger then 3 nm sometimes contained more than two differently oriented smaller regions. Examples of this are shown in Figs. 11a and b for a 4- and a 6-nm particle, respectively. The measured lattice distance in Fig. 11a is 0.232 nm while that in the core of Fig. 11b is 0.256 nm. The arrow in Fig. 11a possibly indicates twin-related regions in the Pd particle.

Heating in Air at 500°C for 24 h

Since no clear indications for the existence of a tetragonal PdO structure were found, some TEM specimens were oxidized in air for 24 h instead of 1 h. In addition to the basic observations described in the previous section, Pd particles larger than 5 nm exhibited a remarkable behavior

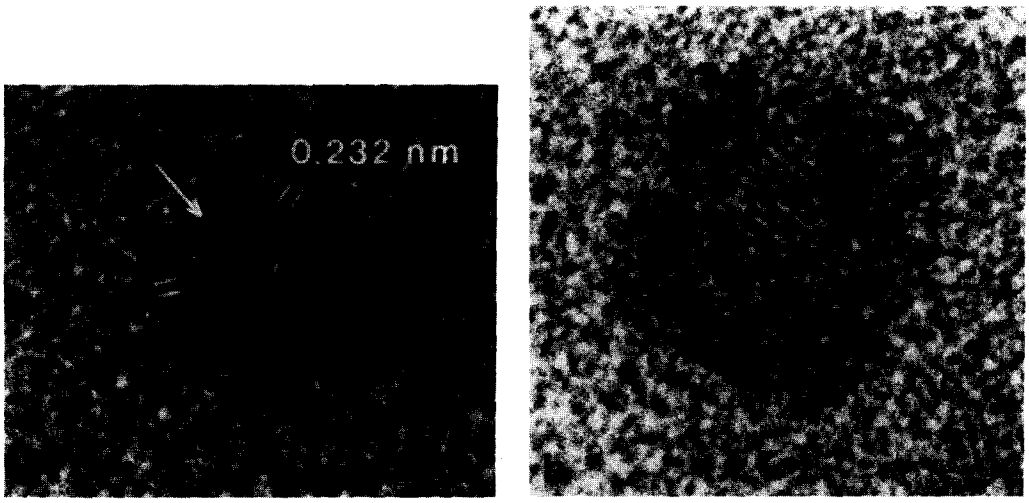

FIG. 11. Multiple orientations in Pd particles (in air at 500°C for 1 h). (a) A 4-nm particle, (b) a 6-nm particle; lattice spacing in the core is 0.256 nm.

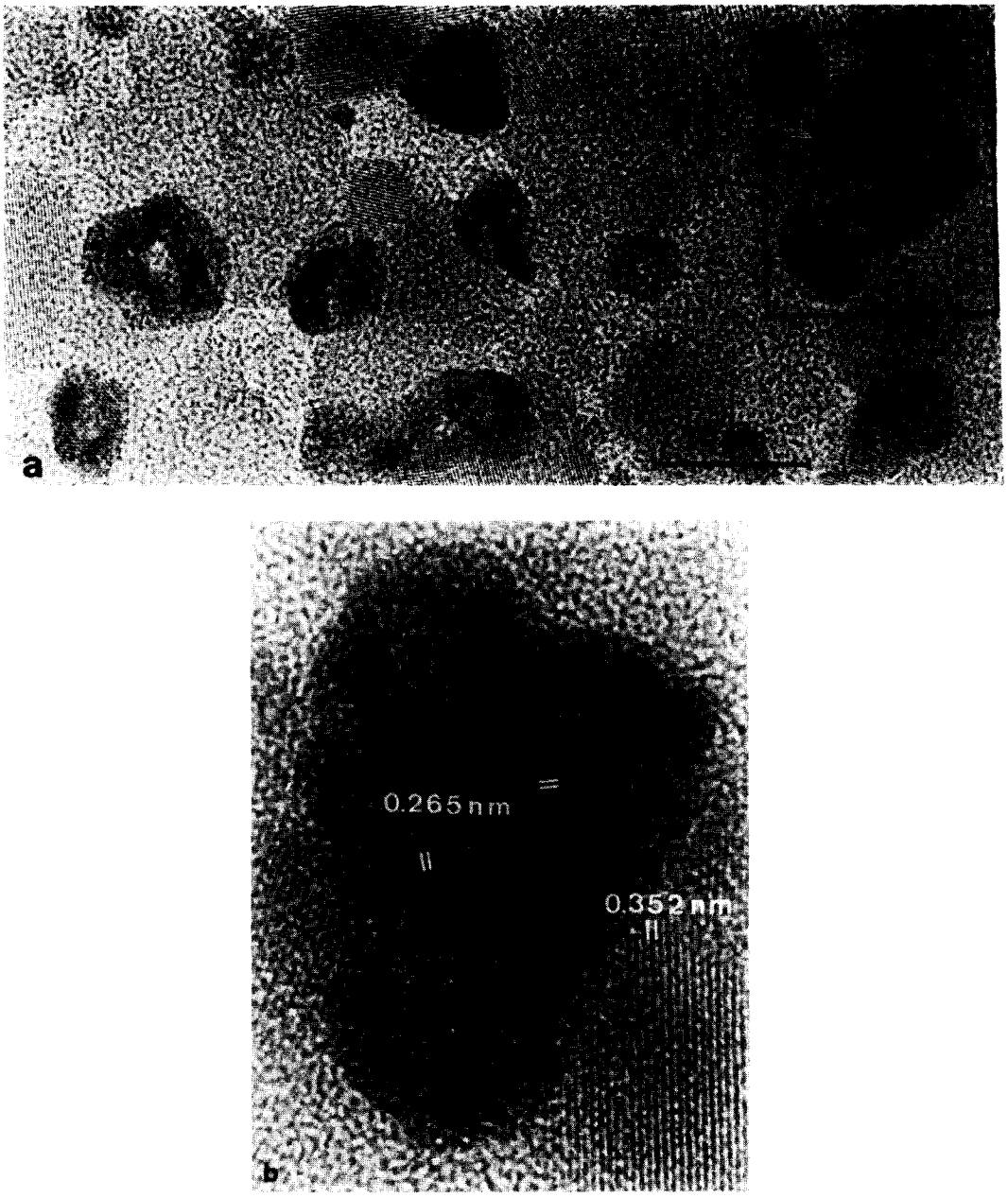

FIG. 12. (a) Pd particles (in air at 500°C for 24 h) showing bright contrast near the center. (b) Higher magnification of Pd particle indicated in (a) showing lattice fringes (interplanar distances 0.265 nm).

which was only slightly revealed in the case of the 1-h oxidation. Figure 12a shows that most of the Pd particles (>5 nm) contain a region near the center where the TEM contrast is brighter than in regions near the edge of the particle. Chen and Ruckenstein reported a similar TEM observation for alumina-supported palladium crystallites which were oxidized in 1 atm of O_2 at temperatures of 350°C and higher (*19*). The ef-

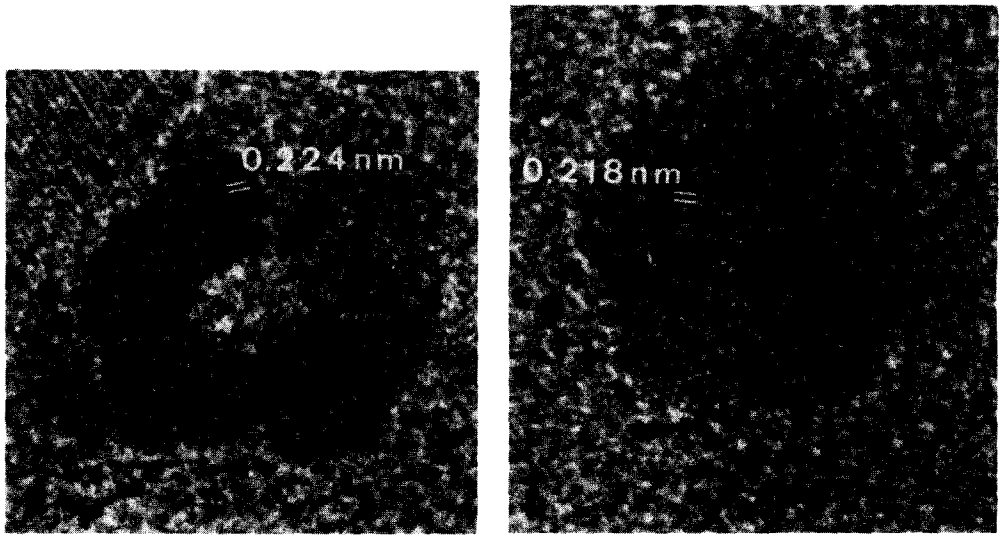

FIG. 13. Differently structured 6-nm Pd particles (in air at 500°C for 24 h). (a) With and (b) without pit in center.

fect was attributed to the formation of pits or cavities in the Pd crystallites and a possible mechanism was given.

Figure 12b, which is a higher magnification of the marked particle in Fig. 12a, contains two regions in which the measured lattice distance is 0.265 nm. This parameter might indicate a PdO structure (bulk PdO: d_{101} = 0.2644 nm (*16*)).

Diverse phenomena occurred during the 24-h oxidation stage and consequently various differently structured Pd particles were observed. To summarize most observations, Figs. 13a and b show two extreme structures of Pd particles. The bright contrast in the center of the 6-nm Pd particle shown in Fig. 13a strongly suggests the presence of a pit. On the other hand, no strong contrast differences are observed in the particle of similar dimensions shown in Fig. 13b. The structures of most other Pd particles can be regarded as intermediates between these two extremes: Pd particles containing a central region with varying size and contrast were observed.

It can be concluded that in our oxidation treatments no particles were produced containing only one stoichiometric PdO phase. If a PdO phase occurs (some evidence is found in Figs. 11b and 12b) it coexists with Pd crystallites.

DISCUSSION

The problem of obtaining quantitative information of atom positions from experimental HREM images is very sensitive to the electron imaging conditions and a local deviation of crystallographic symmetry in the specimen (*20–22*). It is obvious that a large proportion of the metal atoms in small metal particles, which are attached to a crystalline support, are arranged asymmetrically. The presence of a TiO_2–Pd interface, the relatively large amount of surface Pd atoms, an unknown amount of adsorbed or absorbed "impurity" atoms (*23*), and a possible local asymmetric crystallographic configuration around the metal atoms in the interior of the Pd particles may cause complicating anomalies in the HREM images. This, in fact, makes a reliable interpretation of HREM observations of small particles a very difficult task. Unfortunately, the theoretical modeling of lattice image simulations in small metal particles (*24*) is not yet sufficiently advanced to provide research-

ers in the field of catalysts with useful guidelines.

Nevertheless we feel confident that our experimental data reveal some important aspects of heterogeneous metal catalysts, which will now be discussed. The basic experimental observations are the following:

(a) Lattice expansions up to 10% in the non-heated fcc Pd clusters (Figs. 1–3) and up to 15% in Pd clusters heated in air (Figs. 7–11).

(b) The characteristic distortion of the fcc structure (Figs. 7 and 8) and the presence of various lattice defects in the latter (Figs. 9–11).

(c) Indications of an enhanced interfacial interaction between Pd particles and TiO_2 as a result of the heat treatment in air (e.g., Fig. 10).

(d) Possible indications of a PdO structure (Figs. 11b and 12b).

(e) The recrystallization of Pd agglomerates into spherical Pd monocrystallites during heating under HV (Figs. 4 and 6).

Heinemann and Poppa have briefly reviewed TEM studies which deal with lattice contractions or expansions in small metal particles (*25*). Except for the existence of pseudomorphism, none of the mentioned possible explanations for a deviation of the lattice parameters in fcc particles from the bulk value is appropriate to our Pd particles. In particular, we found no indication that might point to the existence of composite crystal structures (*26*) in small Pd particles. The role of epitaxy (*27*) and pseudomorphism (*28*) are currently being investigated. The concept of lattice coincidence is used to derive epitaxial orientations between Pd and TiO_2 (*10*).

The distorted fcc structure cannot be attributed to a temperature-activated interaction between Pd and the inert Si_3N_4 (e.g., Pd silicide formation). This is concluded from a comparison of the different structures obtained in the cases of the HV/heat treatment on the one hand (Figs. 5 and 6) and the air/heat treatment on the other hand (Figs. 7–13).

We assume that the interaction of oxygen with palladium involves the dissociative chemisorption of O_2 on the Pd surface and a subsequent incorporation of oxygen atoms in the bulk of the Pd particles. There is abundant evidence for the existence of dissolved oxygen in Pd (e.g., (*29–32*)) not forming bulk PdO but rather a nonstoichiometric solid phase (a Pd–O alloy). The dissolution of oxygen in Pd already takes place at oxygen pressures far below the dissociation pressure of PdO (*29, 30*). Microcrystallites of stoichiometric tetragonal PdO are formed only when the bulk oxygen concentration attains a critical value (*29*). However, there is some contradiction concerning the experimental conditions under which PdO is formed (*32*). It is generally found that the Pd–O alloy is chemically rather stable and, surprisingly, resists even high-temperature treatments *in vacuo* (*31, 32*).

At this stage we suggest that the distorted fcc structures, which we have observed, represent Pd–O alloys. Absorbed oxygen atoms might be responsible for expanding the fcc lattice and, in a number of particles, might cause a slight deviation of the orientation of the lattice planes. This conclusion is further supported by X-ray diffraction studies of Pt electrodes which had absorbed oxygen due to anodic polarization (*33*). The observed lattice expansions was interpreted as the result of dissolution of oxygen atoms which are interstitially located in the octahedral hole in the center of the unit Pt crystal face center cube (*33, 34*).

The lattice expansion in non-heated fcc clusters can then possibly be explained by a small (room temperature) incorporation of oxygen atoms in the fcc lattice. These oxygen atoms may come from different sources: for example, the laboratory air, the aqueous $PdCl_2$ solution, or, most probably, the oxygen species which are formed in photooxidation/reduction reactions which take place at the TiO_2 surface during photodeposition of Pd (*8*).

The growth of Pd agglomerates by three-

dimensional nucleation is associated with the presence of oxygen atoms on and/or in the Pd clusters (*10*). The oxygen impurities inhibit the recrystallization of the agglomerates into single crystals. The effective recrystallization during heating under HV can be explained by an enhanced mobility of Pd atoms along the grain boundaries due to the (partial) removal of oxygen atoms.

Two other effects, the generation of lattice defects in Pd particles and the enhanced interfacial Pd–TiO_2 interaction, may be connected to the incorporation of oxygen atoms in Pd. The former can intuitively be explained by the non-uniform stresses generated in a Pd particle when (inhomogeneous) volume expansion takes place (*19*). The latter effect is considered to be important in the field of metal–support interactions. There exists considerable experimental evidence for increased interfacial attraction between metals and metal–oxide supports which may be connected with the formation of new metal–oxygen bonds (e.g., (*19, 35, 36*)). However, most observations are only qualitatively understood on the basis of thermodynamic considerations.

Some observations (Figs. 11b and 12b) suggest the surrounding or stabilization of PdO crystallites by Pd–O alloy crystallites. The coexistence of a PdO phase with metal crystallites in one particle has already been proposed by Chen and Ruckenstein (*19*). Moreover, X-ray diffraction studies showed that, during the heating of Pd powders in air, PdO formation already began at 200°C and was only completed at about 700°C (*37*). Our experiments, however, cannot provide unequivocal evidence to clarify the existence of a stoichiometric PdO phase in the reducing vacuum environment of the electron microscope. Two-dimensional lattice images of a PdO lattice, which would definitely have resolved this problem, were not observed.

CONCLUSION

Several interesting structural phenomena associated with the interaction of photodeposited Pd particles on TiO_2 crystallites and ambient oxygen species were revealed by lattice imaging in the Pd particles. This study suggests that in (high-temperature) catalytic reactions the crystallographic structure of small metal particles on inorganic oxide supports may appreciably deviate from a pure fcc structure due to the incorporation of oxygen atoms.

ACKNOWLEDGMENTS

The authors thank J. F. C. M. Verhoeven for preparing Si_3N_4 membranes on Si wafers, Dr. G. J. van der Kolk for carrying out the HV experiments and Prof. S. Amelinckx and Prof. J. Van Landuyt for the use of the equipment of the Electron Microscopy Centre for Materials Research at the University of Antwerp (RUCA).

REFERENCES

1. Grätzel, M., Ed., "Energy Resources through Photochemistry and Catalysis." Academic Press, New York, 1983.
2. Kelly, J. J., and Vondeling, J. K., *J. Electrochem. Soc.* **122,** 1103 (1975).
3. Inoue, T., Fujishima, A., and Honda, K., *J. Electrochem. Soc.* **127,** 1582 (1980).
4. Reiche, H., Dunn, W. W., and Bard, A. J., *J. Phys. Chem.* **83,** 2248 (1979).
5. Koudelka, M., Sanchez, J., and Augustynski, J., *J. Phys. Chem.* **86,** 4278 (1982).
6. Sungbom, C., Kawai, M., and Tanaka, K., *Bull. Chem. Soc. Japan* **57,** 871 (1984).
7. Sato, S., and Kunimatsu, K., *J. Phys. Chem.* **88,** 175 (1984).
8. Jacobs, J. W. M., *J. Phys. Chem.* **90,** in press.
9. Jacobs, J. W. M., and Verhoeven, J. F. C. M., *J. Microsc.* **143,** 103 (1986).
10. Jacobs, J. W. M., to be published.
11. Marks, L. D., and Smith, D. J., *J. Cryst. Growth* **54,** 425, 433 (1981).
12. Marks, L. D., and Smith, D. J., *J. Microsc.* **130,** 249 (1982).
13. Smith, D. J., White, D., Baird, T., and Fryer, J. R., *J. Catal.* **81,** 107 (1983).
14. White, D., Baird, T., Fryer, J. R., Freeman, L. A., Smith, D. J., and Day, M., *J. Catal.* **81,** 119 (1983).
15. Wallenberg, L. R., Bovin, J.-O., and Schmid, G., *Surf. Sci.* **156,** 256 (1985).
16. TiO_2: ASTM file 21-1272; Pd: ASTM file 5-0681; PdO: ASTM file 6-0515.
17. Van Dyck, D., Van Tendeloo, G., and Amelinckx, S., *Ultramicroscopy* **15,** 357 (1984).

18. Coene, W., Bender, H., Lovey, F. C., Van Dyck, D., and Amelinckx, S., *Phys. Status Solidi A* **87,** 483 (1985).
19. Chen, J. J., and Ruckenstein, E., *J. Phys. Chem.* **85,** 1606 (1981).
20. Self, P. G., Glaisher, R. W., and Spargo, A. E. C., *Ultramicroscopy* **18,** 49 (1985).
21. Marks, L. D., *Surf. Sci.* **139,** 281 (1984).
22. Saxton, W. O., and Smith, D. J., *Ultramicroscopy* **18,** 39 (1985).
23. Fromm, E., and Hörz, G., *Int. Metals Rev.* **25,** 269 (1980).
24. Marks, L. D., *Ultramicroscopy* **18,** 445 (1985).
25. Heinemann, K., and Poppa, H., *Surf. Sci.* **156,** 265 (1985).
26. Yang, C. Y., *J. Cryst. Growth* **47,** 274 (1979).
27. Takayanagi, K., Yagi, K., and Honjo, G., *Thin Solid Films* **48,** 137 (1978).
28. Heinemann, K., Osaka, T., Poppa, H., and Avalos-Borja, M., *J. Catal.* **83,** 61 (1983).
29. Campbell, C. T., Foyt, D. C., and White, J. M., *J. Phys. Chem.* **81,** 491 (1977).
30. Close, J. S., and White, J. M., *J. Catal.* **36,** 185 (1975).
31. Conrad, H., Ertl, G., Küppers, J., and Latta, E. E., *Surf. Sci.* **65,** 245 (1977).
32. Surnev, L., Bliznakov, G., and Kiskinova, M., *Surf. Sci.* **140,** 249 (1984).
33. Hoare, J. P., Meibuhr, S. G., and Thacker, R., *J. Electrochem. Soc.* **113,** 1078 (1966); **116,** 612, 1390 (1969).
34. Hoare, J. P., *Electrochim. Acta* **26,** 225 (1981); **27,** 1751 (1982).
35. Klomp, J. T., *J. Phys.*, in press.
36. Huizinga, T., Thesis, University of Technology, Eindhoven (1983), Chapter 1 and references therein.
27. Bayer, G., and Wiedemann, H. G., *Thermochim. Acta* **11,** 79 (1975).